Chemosensors **2015**, *3*, 241-252; doi:10.3390/chemosensors3040241

OPEN ACCESS

Chemosensors

ISSN 2227-9040

www.mdpi.com/journal/chemosensors

Article

Selectivity of Catalytically Modified Tin Dioxide to CO and NH_3 Gas Mixtures

Artem Marikutsa *, Marina Rumyantseva and Alexander Gaskov

Chemistry Department, Moscow State University, Vorobyevy gory 1-3, Moscow 119991, Russia; E-Mails: roum@inorg.chem.msu.ru (M.R.); gaskov@inorg.chem.msu.ru (A.G.)

***** Author to whom correspondence should be addressed; E-Mail: artem.marikutsa@gmail.com; Tel.: +7-495-939-5471; Fax: +7-495-939-0998.

Academic Editor: Russell Binions

Received: 2 September 2015 / Accepted: 28 September 2015 / Published: 9 October 2015

Abstract: This paper is aimed at selectivity investigation of gas sensors, based on chemically modified nanocrystalline tin dioxide in the detection of CO and ammonia mixtures in air. Sol-gel prepared tin dioxide was modified by palladium and ruthenium oxides clusters via an impregnation technique. Sensing behavior to CO, NH_3 and their mixtures in air was studied by *in situ* resistance measurements. Using the appropriate match of operating temperatures, it was shown that the reducing gases mixed in a ppm-level with air could be discriminated by the noble metal oxide-modified SnO_2. Introducing palladium oxide provided high CO-sensitivity at 25–50 ℃. Tin dioxide modified by ruthenium oxide demonstrated increased sensor signals to ammonia at 150–200 ℃, and selectivity to NH_3 in presence of higher CO concentrations.

Keywords: gas mixture analysis; selectivity; gas sensors; nanocrystalline tin dioxide; surface modification; carbon monoxide; ammonia

1. Introduction

Lack of selectivity is a major drawback of semiconductor metal oxide gas sensors. Nanocrystalline tin dioxide is one of the most utilized materials for such devices due to a combination of appropriate structural, adsorptive, and electrophysical properties [1]. The material, possessing several advantages, such as large active surface area and surface-to-volume ratio, result in high gas sensitivity, stability in

air, and low cost, makes it challenging to improve selectivity [2]. The problem of selectivity is complicated by the fact that most toxic gases (CO, NH_3, H_2S, volatile organic compounds) are the reducing ones. The sensor response to these gases is determined by the molecules oxidation on the material surface.

There are several tools to improve the sensitivity and selectivity of the detection of reducing gases. These include modulation of temperature regime of sensors operation, such as pulsed-temperature [3] or cycled-temperature regime [4]. Another approach is the modulation of the sensor measurement principle. For example, measuring voltage fluctuations instead of DC-resistance of nanocrystalline Pd_xWO_3-based sensors was shown to be hundreds of times more sensitive to the presence of ethanol vapor [5]. In environmental applications there is the need to selectively detect traces of reducing gases mixed in air, e.g., to discriminate toxic, fire alarming gases, food quality indicators, disease markers, *etc.* [6]. A promising tool to meet this challenge is the development of artificial olfaction systems (electronic nose). Such systems are based on a network of sensors operated in similar or different temperature modes. The treatment of multidimensional data from sensors networks requires a pattern recognition algorithm, such as principal component analysis [6]. In a recent review by Seifert *et al.*, new mathematic algorithms for calibration and pattern recognition of sensor networks were demonstrated, the procedures being efficient for components concentration evaluation in gas mixtures composed of volatile organic compounds [7]. The operation temperature regime is also important in sensors networks: it was established that ammonia leakages could be selectively detected in the presence of water vapor, using commercial tin dioxide-based sensors operated in a linear heating–cooling mode [8]. On the other hand, in multisensory networks, it is reasonable to combine sensors with specific sensitivities to target gases. In this case, the "orthogonal" data from different sensors would be beneficial for the detection of various target gases and reliable discrimination of their mixtures. Thus, improving sensing materials' selectivities is a challenge, not only for individual gas sensors, but also for sensor network systems.

An efficient approach to improve the selectivity of a gas sensing material is the chemical modification of a semiconductor oxide [2,9]. Catalytic additives of noble metals have been established as efficient modifiers, enhancing sensitivity and selectivity to reducing gases, e.g., to CO the efficient modifiers are Pd [10–13], Au [14,15], Pt [16]; to H_2S—CuO [17]; to NH_3—RuO_2 [18]; to LPG—Pd [19], Au [20]. However, the appropriate choice of a modifier is a non-trivial issue, since in the complex process of gas sensing not only the catalytic activity of clusters, but also their interference with the oxide surface sites, defines the sensor characteristics of modified material [21,22]. In our recent works, we demonstrated that nanocrystalline tin dioxide modification by palladium oxide increased sensor responses to CO at as low temperature as room temperature [23]; while introducing ruthenium oxide provided high responses to NH_3 at a raised temperature [24]. However, these studies dealt with individual gases. The specific sensitization to CO and NH_3 motivated an interest to appreciate whether the catalytic additives bring about enough selectivity to allow for distinguishing these reducing gases mixed together in a ppm-concentration level.

In the present work, the cross-sensing behavior of nanocrystalline SnO_2 modified by palladium and ruthenium oxides to CO + NH_3 gas mixtures in air was studied to estimate the selectivity.

2. Experimental Section

Nanocrystalline SnO_2, SnO_2/PdO_x, and SnO_2/RuO_y materials were used for the study. Tin dioxide was synthesized using the aqueous ammonia-assisted sol-gel route [23]. 0.3 M solution of tin (IV) chloride in deionized water was obtained using $SnCl_4 \cdot 5H_2O$ (>99% pure, Sigma-Aldrich). 1 M ammonia solution was rapidly added until pH 6 was reached, after that, the deposit of α-stannic acid was left for 1 h at room temperature. Next, it was separated by centrifugation and washed several times with deionized water to remove chloride-ions (check by $AgNO_3$ solution). The washed $SnO_2 \cdot nH_2O$ deposit was dried at 50 °C overnight and annealed in air at 300 °C for 24 h. Chemical modification of nanocrystalline tin dioxide by 1 wt.% of PdO_x or RuO_y was performed via the impregnation of as-obtained SnO_2 powder by ethanol solution of noble metal acetylacetonate precursors. The impregnated samples, $SnO_2/Pd(acac)_2$ and $SnO_2/Ru(acac)_3$, were calcined at 225 °C and 265 °C, respectively, to decompose the modifier precursors at a sufficiently lower temperature [25,26].

The concentration of noble metal modifiers was measured by ICP-assisted analysis using a quadruple mass-spectrometer 7500c ("Agilent"). For this purpose, the powders were alloyed with zinc and then dissolved in nitric acid under heating. The measurements were performed for five isotopes of each modifier, and the signal were registered at mass numbers: for Pd at 104, 105, 106, 108, 110; and for Ru at 96, 98, 100, 101, 102. The micrographs of the nanocomposites were obtained using high-resolution transmission electron microscopy (HRTEM), high angle annular dark field scanning transmission electron microscopy (HAADF-STEM), and energy-dispersive X-ray (EDX) analysis with a Tecnai G2 transmission electron microscope operated at 200 kV. Characterization of the samples by X-ray diffraction (XRD), electron diffraction (ED), X-ray absorption spectroscopy (XANES and EXAFS), X-ray photoelectron spectroscopy (XPS), and electron paramagnetic resonance (EPR) were described in our previous publications [23–27]. The composition and microstructure parameters of the samples are summarized in Table 1.

Sensor tests were performed by *in situ* measurements of the sensors' DC-resistance at temperatures in the range of 25–250 °C and with controlled gas composition. To prepare the sensors, the sample powders were mixed with a binder (terpeniol). The paste was thick film-deposited onto alumina microelectronic hotplates, which provided vapor-deposited rectangular-shaped Pt contacts (0.3 × 0.2 mm) separated by a 0.2 mm gap and with embedded Pt-heaters. The sensing layer (5–7 micrometres thick) covered an area of 1.0 × 0.5 mm. The sensors were placed in the gas-purged (100 mL/min) chamber of a resistance-measuring device. Before measurements, the sensors were annealed at 200 °C for 14 h under purified air to remove the binder and to clean the surface from atmospheric impurities. Test gas was purged through the chamber in a pulsed regime: background gas–test gas–background gas. A purified air generator (model 1,2-3,5, "Himelectronica", Russia) was used as the source of the background gas; the contaminations level is not exceeding: 10 ppm H_2O, 2 ppm CO_2, 0.1 ppm hydrocarbons. The test gas sources were certified gas mixtures ("Linde-Gas", Moscow, Russia): CO (517 ± 12 ppm): N_2 and NH_3 (209 ± 8 ppm): air. Exposure time in test gas was 15 min, recovery time in air was 30 min. The cycled target gas exposure was performed three to four times for reproducibility. The concentrations of analytes were 2–50 ppm CO and 0.4–50 ppm NH_3 in the analyses of individual gases. The dilution of target gases in purified air was performed using mass-flow controllers ("Bronkhorst"). The sensor signal was defined as a ratio of sensor resistance in background gas (R_{air}) to that in test gas (R_{gas}):

$$S = R_{air}/R_{gas} \quad (1)$$

For selectivity tests, the mixtures of CO + NH_3 with component concentrations, varied in the range of 5–20 ppm in air, were prepared. Sensors were operated at constant temperatures, corresponding to the maximum sensitivity to individual gases: SnO_2 at 250 °C, SnO_2/PdO_x at 50 °C, and SnO_2/RuO_y at 200 °C.

3. Results and Discussion

3.1. Materials Composition and Microstructure

As was shown by diffraction techniques (Table 1), the samples contain one crystalline phase of cassiterite (SnO_2), with an average crystallite size of 3–6 nm. Due to small concentrations, the additives could not be detected by XRD or ED. Using XPS, XANES, EXAFS, and EPR, the modifiers were shown to exist in the form of mixed-valence noble metal oxides, which could be formalized as PdO_x and RuO_y, respectively. The techniques allowed estimation of the fractions of different oxidation states of palladium and ruthenium in the nanocomposites (Table 1). The total concentration of Pd and Ru, measured by ICP-mass spectrometry, is close to the loaded amount of 1 wt.%. The additives could not be visualized on HRTEM images (Figure 1), presumably due to close atomic numbers with Sn, and, hence, close contrast with the support on the electronic micrographs. Using EDX-mapping with HAADF-STEM, the modifiers were observed in the form of clusters on the surface of agglomerated tin dioxide nanoparticles (Figure 2a,b). The size of PdO_x and RuO_y clusters were estimated at 1–5 nm, while those of aggregates of tin dioxide particles reached 20–80 nm. Previously, we demonstrated micrographs of PdO_x clustered on SnO_2 crystallites with a size of more than 50 nm (tin dioxide annealed at 700 °C) that was detectable by HRTEM [27].

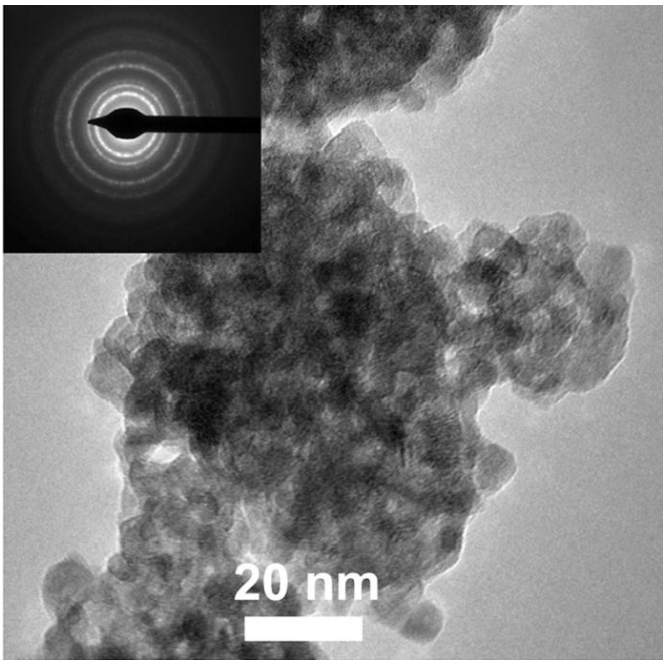

Figure 1. HRTEM micrograph of SnO_2/PdO_x sample; inset—electron diffraction pattern.

Table 1. Materials composition and microstructure parameters.

Sample	Crystalline Phase [a]	Modifier Content and Composition		Particle Size, nm			BET Area, m^2/g
		Total Concentration [b], wt.%	Oxidation and Crystalline State [c], at.% from Total Modifier Concentration	SnO_2		Modifier [e]	
				(d_{XRD})[a]	(d_{TEM})[d]		
SnO_2	SnO_2			3–6	2–8		95–100
SnO_2/PdO_x		0.94 ± 0.05	70 at.%—PdO (amorphous) 25 at.%—Pd^0 5 at.%—Pd^{3+}	3–5		1–3	90–95
SnO_2/RuO_y		0.81 ± 0.05	80 at.%—RuO_2 (structured) 20 at.%—Ru^{3+}	3–5		2–5	90–95

[a] According to XRD and electron diffraction [23,24,26,27];
[b] from ICP-mass spectrometry analysis;
[c] estimated by XANES, EXAFS, XPS and EPR [23–25,27],
[d] from HRTEM;
[e] evaluated by HAADF-STEM and EDX-mapping.

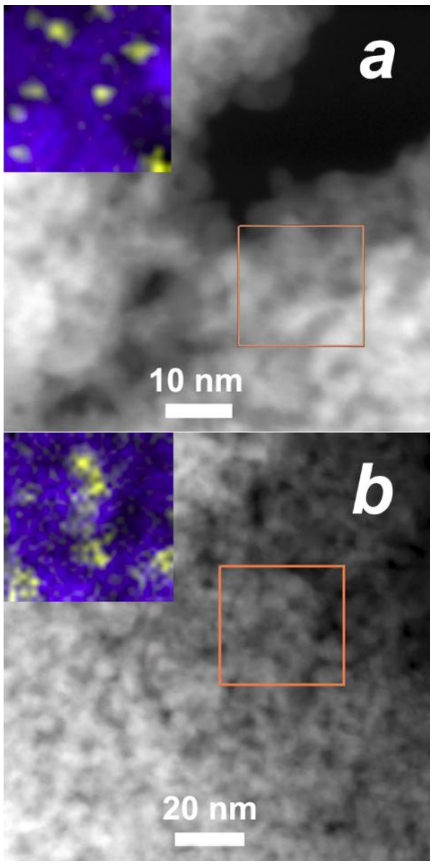

Figure 2. HAADF-STEM images of (**a**) SnO_2/PdO_x and (**b**) SnO_2/RuO_y samples; inset—EDX maps of selected areas (blue—Sn, yellow—noble metal).

3.2. Sensing Behavior to Individual CO and NH_3 Gases

The influence of PdO_x and RuO_y catalytic clusters on the sensitivity of nanocrystalline tin dioxide to CO and NH_3 was compared from the sensing tests to individual gases. Figures 3 and 4 illustrate the dynamic resistance response of SnO_2, SnO_2/PdO_x, and SnO_2/RuO_y sensors to 50 ppm of CO or NH_3 at variable operating temperatures of 25–250 ℃. The highest responses to CO were observed for PdO_x-modified tin dioxide in the whole temperature range (Figure 3). At a lower temperature region (25–50 ℃), the sensitivity of SnO_2/PdO_x increased, however, the response kinetics were poor: the recovery time, *i.e.*, time needed to reach 90% of resistance value in air (R_{air}) when the target gas is switched off, increased from τ_{90} ~ 10 min at T = 200 ℃ to τ_{90} ~ 25 min at room temperature.

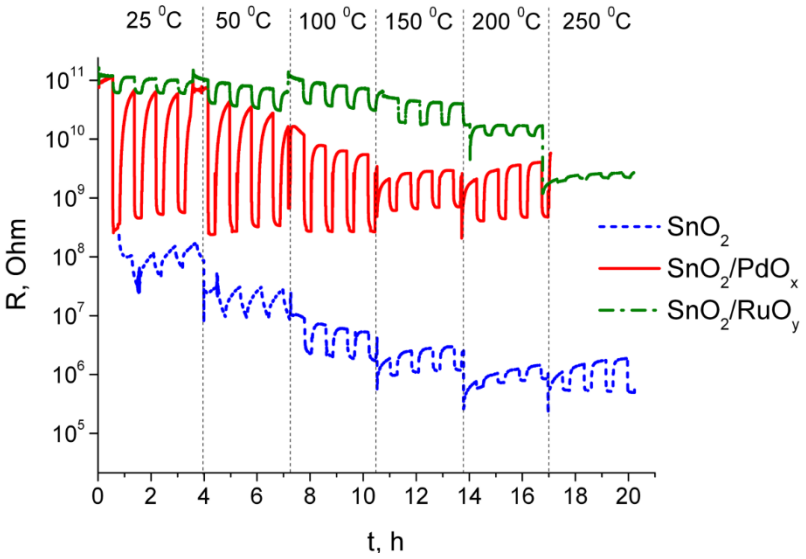

Figure 3. Dynamic resistance response of SnO_2, SnO_2/PdO_x, and SnO_2/RuO_y sensors to the pulses of 50 ppm CO in air at different temperatures.

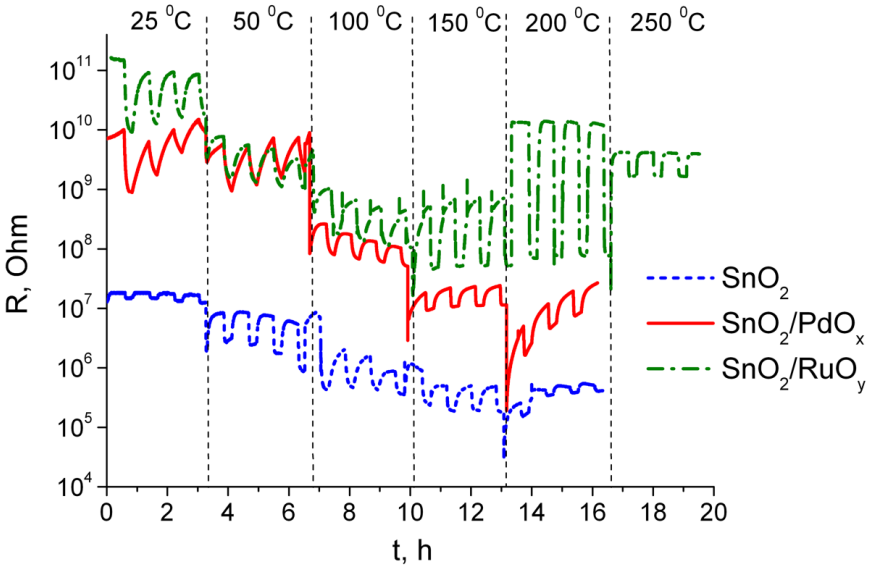

Figure 4. Dynamic resistance response of SnO_2, SnO_2/PdO_x, and SnO_2/RuO_y sensors to the pulses of 50 ppm NH_3 in air at different temperatures.

The response of SnO_2/PdO_x to 50 ppm NH_3 was low and unstable, especially at low temperature (Figure 4). Low responses with long response (τ_{90} > 10 min) and recovery (τ_{90} > 25 min) time were characteristic for all the sensors when detecting NH_3 at T = 25–50 ℃. Raising the operating temperature resulted in the increase of sensitivity to NH_3, most prominently for SnO_2/RuO_y sensor (Figure 4). Corresponding sensor signals to 50 ppm of CO and NH_3, calculated via Equation (1), are plotted in Figures 5 and 6, respectively, as a function of operating temperature. SnO_2/PdO_x demonstrated the highest sensor signals to CO compared to other samples, with the maximum at T = 25–50 ℃ (Figure 5). SnO_2/RuO_y was characterized by superior signals to ammonia, with the maximum at T = 200 ℃ (Figure 6). Since the samples are characterized by quite close particle sizes and BET area values (Table 1), the sensitization effects are due to the influence of catalytic modifiers on the interaction of materials' surfaces with target gas molecules, rather than their affecting the materials' microstructure. Recently, we reported on the specific promoting effect of PdO_x and RuO_y clusters on the active sites on the surface of nanocrystalline tin dioxide [28]. This should be an important factor controlling the specificity of materials' interaction with gases.

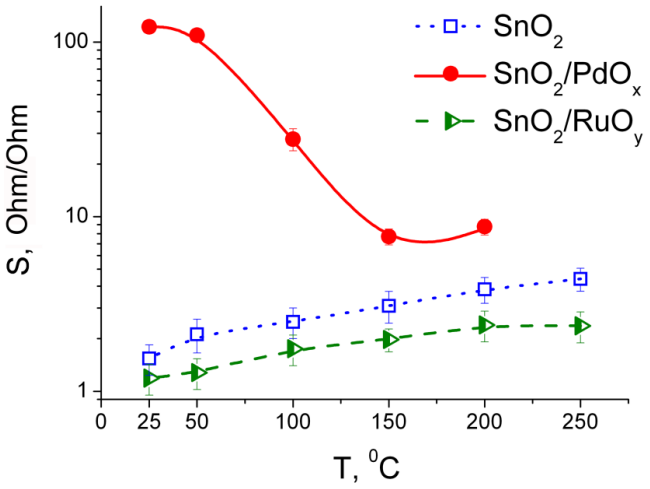

Figure 5. Temperature dependence of sensor signals of nanocrystalline SnO_2, SnO_2/PdO_x, and SnO_2/RuO_y samples to 50 ppm CO.

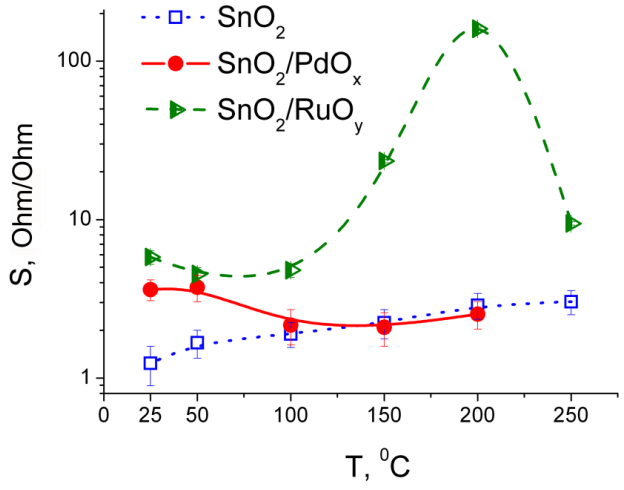

Figure 6. Temperature dependence of sensor signals of nanocrystalline SnO_2, SnO_2/PdO_x, and SnO_2/RuO_y samples to 50 ppm NH_3.

3.3. Sensing Behavior to CO + NH_3 Gases Mixtures

To estimate the selectivity of the catalytically-modified tin dioxide sensing test to gas mixtures of CO + NH_3 was performed. The upper plot in Figure 7 shows the dynamic resistance responses of the sensors to target gas mixtures with different component concentrations. During the measurements, the sensors were operated at temperatures appropriate for the specific detection of corresponding molecules, which were chosen based on the above-discussed temperature profiles of sensor signals (Figures 5 and 6). SnO_2/PdO_x was operated at 50 ℃ to detect CO in the mixture, SnO_2/RuO_y at 200 ℃ for specific NH_3 sensing. Blank SnO_2, the sensitivity of which unselectively increased with temperature, was operated at 250 ℃ as a reference sensor. The experiment was carried out so that, firstly, CO (20 ppm) pulses were purged through the chamber. Subsequently, an increasing concentration of NH_3 (5–10–20 ppm) was admixed to the test gas containing 20 ppm CO. Finally, NH_3 concentration was fixed at 20 ppm and CO content was decreased step-by-step to 10–5–0 ppm. Corresponding sensor signals to test gas mixtures were calculated using Equation (1) and are plotted in the lower part of Figure 7.

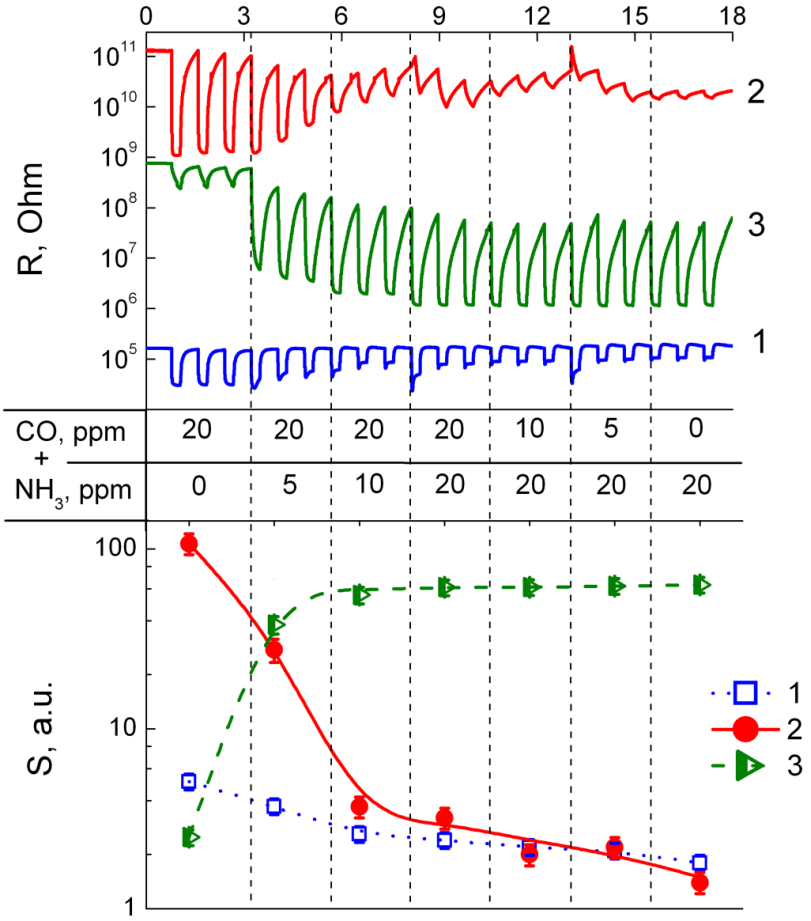

Figure 7. Upper plot: dynamic resistance response of SnO_2 (1), SnO_2/PdO_x (2), and SnO_2/RuO_y (3) sensors to the pulses of CO + NH_3 mixtures in air. The component concentrations in the test gas mixture are shown in the middle table. Operating temperature of sensors: SnO_2—250 ℃, SnO_2/PdO_x—50 ℃, SnO_2/RuO_y—200 ℃. Lower plot: corresponding sensor signals to the test gas mixtures.

As can be seen in Figure 7, the SnO_2/RuO_y sensor displayed extremely low responses to 20 ppm CO. However, introducing a lower concentration of NH_3 (5 ppm) to the test gas mixture resulted in a drastic sensor signal growth, increasing further with the increase of NH_3 concentration. Decreasing the concentration of CO affected, neither response behavior, nor the sensor signal values of SnO_2/RuO_y (Figure 7). Hence, SnO_2/RuO_y is selective to ammonia in comparison with CO when the gases are mixed in a ppm-concentration level with air. Previously, the additive of RuO_y was found to promote oxygen spillover and dissociation on the surface of SnO_2/RuO_y to a larger extent than on SnO_2 or SnO_2/PdO_x [27]. This resulted in the highest promotion of oxygen species on the surface of SnO_2/RuO_y, comparing to other samples [28]. These oxygen species could be the active sites for ammonia oxidation at raised temperatures. However, since surface oxygen species are unselective to reducing gases, the main reason for SnO_2/RuO_y–NH_3 selectivity should be the specific catalysis of ammonia oxidation. In a recent work, we established catalytic role of RuO_y clusters in deep NH_3 oxidation to nitrogen oxides as the main feature reflecting increased sensitivity of SnO_2/RuO_y to ammonia at raised temperatures [24]. In contrast to that, ammonia is likely oxidized to N_2 on the surface of PdO_x-modified or blank SnO_2.

The SnO_2/PdO_x sensor demonstrated highest responses to 20 ppm CO when there was no ammonia in the test gas (Figure 7). The addition of as little as 5 ppm NH_3 resulted in a sensor signal decrease, despite the persistence of a CO concentration (20 ppm). This effect increased as a higher concentration of ammonia was added to the gas mixture. A similar behavior was observed for blank SnO_2-based sensor, but the NH_3-induced sensor signal depression was less prominent in this case (Figure 7). It suggests that interaction of tin dioxide with CO, and the sensitization provided by PdO_x clusters at low temperatures, proceed via a different mechanism in comparison to the SnO_2/RuO_y-NH_3 interaction at raised temperatures. Direct CO oxidation by surface OH-groups on the surface of SnO_2/Pd, facilitated by the catalytic additive, was discovered in the works of Barsan *et al.* [21]. We proposed that CO interaction with surface hydroxyls is responsible for increased SnO_2/PdO_x sensitivity to carbon oxide at temperatures as low as room temperature [23]. Moreover, it was PdO_x that, to the largest extent, promoted tin dioxide surface hydroxylation by increasing the concentration of different hydroxyl species, including reactive ones, such as Broensted acid sites, paramagnetic OH·, and hydrogen-bonded OH…OH groups [28]. In this respect, the inhibition of SnO_2/PdO_x sensitivity to a fixed (20 ppm) CO concentration by adding even a smaller concentration of ammonia (5 ppm) can be attributed to blocking surface OH-groups by chemisorbed ammonia. Furthermore, the low operating temperature of the SnO_2/PdO_x sensor (50 ℃) is favorable for the adsorption of basic NH_3 molecules on Broensted acid sites, *i.e.*, on surface hydroxyl species.

In this context, the sensors' operation at low temperatures has limited applicability for environmental monitoring. Moreover, ambient humidity would block the active sites for CO oxidation, as well as ammonia gas in the above-discussed situation with SnO_2/PdO_x and SnO_2. However, we believe that the specific sensitivities of the studied materials might be advantageous for the use of the sensors (as a future prospect) in multisensory devices. In the work of Frank *et al.*, it was shown that using sensor networks, based on tin dioxide with different additives (palladium oxide, cobalt oxide, copper oxide, *etc*.), the realization of the selective analysis of hydrocarbons gas mixtures could be achieved [29]. Perhaps, the selectivity of CO and ammonia detection in gas mixtures could benefit from the strong distinction of the temperature dependence of sensitivity in the SnO_2/PdO_x-CO (Figure 5) and SnO_2/RuO_y–NH_3 systems (Figure 6). The issue of sensor surface poisoning at low temperatures could be overcome by an

appropriate modulation of the operating temperature, e.g., pulsed heating to desorb impurities or applying a temperature gradient to the sensing layers [4,29]. However, this is a matter for further research with these materials.

4. Conclusions

Modification of nanocrystalline SnO_2 using palladium and ruthenium oxides results in gas sensitivity increase to CO at low temperatures (25–50 °C) and to NH_3 at a raised temperature (150–200 °C), respectively. A selectivity test for the detection of CO + NH_3 gas mixtures with air revealed that SnO_2/RuO_y is selective to NH_3 in the presence of higher CO concentrations. The selectivity is supposed to arise from RuO_y-catalyzed oxidation of NH_3 to nitrogen dioxide. CO sensing by PdO_x-modified tin dioxide at low temperatures is likely to involve target molecules oxidation by surface OH-groups, which are promoted by the modifier. CO sensitivity of SnO_2/PdO_x is suppressed by lower ammonia concentrations in gas mixtures due to the inhibition of active surface hydroxyls by NH_3 chemisorption, favored by low operating temperatures.

Acknowledgments

The authors acknowledge the Russian Science Foundation (grant 14-19-00120) for financial support.

Author Contributions

Artem Marikutsa and Marina Rumyantseva contributed equally to the experimental work and discussion of the results. Alexander Gaskov contributed greatly to the concept, purposing of the work, and discussion of the results.

Conflicts of Interest

The authors declare no conflicts of interest.

References

1. Batzill, M.; Diebold, U. The surface and materials science of tin oxide. *Prog. Surf. Sci.* **2005**, *79*, 47–154.
2. Korotcenkov, G. Gas response control through structural and chemical modification of metal oxide films: state of the art and approaches. *Sens. Actuators B Chem.* **2005**, *107*, 209–232.
3. Samotaev, N.N.; Vasiliev, A.A.; Podlepetsky, B.I.; Sokolov, A.V.; Pisliakov, A.V. The mechanism of the formation of selective response of semiconductor gas sensor in mixture of CH_4/H_2/CO with air. *Sens. Actuators B Chem.* **2007**, *127*, 242–247.
4. Frank, K.; Kohler, H.; Guth, U. Influence of the measurement conditions on the sensitivity of SnO_2 gas sensors operated thermo-cyclically. *Sens. Actuators B Chem.* **2009**, *141*, 361–369.
5. Ederth, J.; Smulko, J.M.; Kish, L.B.; Heszler, P.; Granqvist, C.G. Comparison of classical and fluctuation-enhanced gas sensing with Pd_xWO_3 nanoparticle films. *Sens. Actuators B Chem.* **2006**, *113*, 310–315.

6. Pearce T.C.; Schiffman, S.S.; Nagle H.T.; Gardner, J.W. *Handbook of Machine Olfaction: Electronic Nose Technology*; Weinheim: Wiley, Weinheim, Germany, 2003.
7. Seifert, R.; Keller, H.; Matthes, J. A review on innovative procedures for the analysis of data from gas sensor systems and networks. *Sens. Transducers* **2015**, *184*, 1–10.
8. Jerger, A.; Kohler, H.; Becker, F.; Keller, H.B.; Seifert, R. New applications of tin oxide gas sensors II. Intelligent sensor system for reliable monitoring of ammonia leakages. *Sens. Actuators B Chem*. **2002**, *81*, 301–307.
9. Rumyantseva, M.N.; Gaskov, A.M. Chemical modification of nanocrystalline metal oxides: Effect of the real structure and surface chemistry on the sensor properties. *Rus. Chem. Bull.* **2008**, *57*, 1106–1125.
10. Cabot, A.; Arbiol, J.; Morante, J.R.; Weimar, U.; Barsan, N.; Gopel, W. Analysis of the noble metal catalytic additives introduced by impregnation of as obtained SnO_2 sol–gel nanocrystals for gas sensors. *Sens. Actuators B Chem*. **2000**, *70*, 87–100.
11. Yuasa, M.; Masaki, T.; Kida, T.; Shimanoe, K.; Yamazoe, N. Nano-sized PdO loaded SnO_2 nanoparticles by reverse micelle method for highly sensitive CO gas sensor. *Sens. Actuators B Chem*. **2009**, *136*, 99–104.
12. Aruna, I.; Kruis, F.E.; Kundu, S.; Muhler, M.; Theissmann, R.; Spasova, M. CO ppb sensors based on monodispersed SnO_x: Pd mixed nanoparticle layers: Insight into dual conductance response. *J. Appl. Phys.* **2009**, doi:10.1063/1.3097470.
13. Kim, B.; Lu, Y.J.; Hannon, A.; Meyyappan, M.; Li, J. Low temperature Pd/SnO_2 sensor for carbon monoxide detection. *Sens. Actuators B Chem*. **2013**, *177*, 770–775.
14. Manjula, P.; Arunkumar, S.; Manorama, S.V. Au/SnO_2 an excellent material for room temperature carbon monoxide sensing. *Sens. Actuators B Chem*. **2011**, *152*, 168–175.
15. Hubner, M.; Koziej, D.; Grunwaldt, J.-D.; Weimar, U.; Barsan, N. An Au clusters related spill-over sensitization mechanism in SnO_2-based gas sensors identified by operando HERFD-XAS, work function changes, DC resistance and catalytic conversion studies. *Phys. Chem. Chem. Phys.* **2012**, *14*, 13249–13254.
16. Ramgir, N.S.; Hwang, Y.K.; Jhung, S.H.; Mulla, I.S.; Chang, J.-S. Effect of Pt concentration on the physicochemical properties and CO sensing activity of mesostructured SnO_2. *Sens. Actuators B Chem*. **2006**, *114*, 275–282.
17. Vasiliev, R.B.; Rumyantseva, M.N.; Yakovlev, N.V.; Gaskov, A.M. CuO/SnO_2 thin film heterostructures as chemical sensors to H_2S. *Sens. Actuators B Chem.* **1998**, *50*, 186–193.
18. Wagh, M.S.; Jain, G.H.; Patil, D.R.; Patil, S.A.; Patil, L.A. Modified zinc oxide thick film resistors as NH_3 gas sensor. *Sens. Actuators B Chem.* **2006**, *115*, 128–133.
19. Srivastava, J.K.; Pandey, P.; Mishra, V.N.; Dwivedi, R. Sensing mechanism of Pd-doped SnO_2 sensor for LPG detection. *Solid State Sci.* **2009**, *11*, 1602–1605.
20. Mishra, V.N.; Agarwal, R.P. Sensitivity, response and recovery time of SnO_2 based thick-film sensor array for H_2, CO, CH_4 and LPG. *Microelectron. J.* **1998**, *29*, 861–874.
21. Barsan, N.; Weimar, U. Understanding the fundamental principles of metal oxide based gas sensors; the example of CO sensing with SnO_2 sensors in the presence of humidity. *J. Phys. Condens. Matter* **2003**, *15*, 813–839.

22. Menini, P.; Parret, F.; Guerrero, M.; Soulantica, K.; Erades, L.; Maisonnat, A.; Chaudret, B. CO response of a nanostructured SnO_2 gas sensor doped with palladium and platinum. *Sens. Actuators B Chem.* **2004**, *103*, 111–114.
23. Marikutsa, A.V.; Rumyantseva, M.N.; Yashina, L.V.; Gaskov, A.M. Role of surface hydroxyl groups in promoting room temperature CO sensing by Pd-modified nanocrystalline SnO_2. *J. Solid State Chem.* **2010**, *183*, 2389–2399.
24. Marikutsa, A.V.; Krivetskiy, V.; Yashina, L.V.; Rumyantseva, M.; Konstantinova, E.A.; Ponzoni, A.; Comini, E.; Abakumov, A.; Gaskov, A.M. Catalytic impact of RuO_x clusters to high ammonia sensitivity of tin dioxide. *Sens. Actuators B Chem.* **2012**, *175*, 186–193.
25. Marikutsa, A.V.; Rumyantseva, M.N.; Gaskov, A.M.; Konstantinova, E.A.; Grishina, D.A.; Deygen, D.M. CO and NH_3 sensor properties and paramagnetic centers of nanocrystalline SnO_2 modified by Pd and Ru. *Thin Solid Films* **2011**, *520*, 904–908.
26. Frolov, D.D.; Kotovshchikov, Y.N.; Morozov, I.V.; Boltalin, A.I.; Fedorova, A.A.; Marikutsa, A.V.; Rumyantseva, M.N.; Gaskov, A.M.; Sadovskaya, E.M.; Abakumov, A.M. Oxygen exchange on nanocrystalline tin dioxide modified by palladium. *J. Solid State Chem.* **2012**, *186*, 1–8.
27. Marikutsa, A.V.; Rumyantseva, M.N.; Frolov, D.D.; Morozov, I.V.; Boltalin, A.I.; Fedorova, A.A.; Petukhov, I.; Yashina, L.V.; Konstantinova, E.A.; Sadovskaya, E.M.; *et al*. Role of PdO_x and RuO_y clusters in oxygen exchange between nanocrystalline tin dioxide and the gas phase. *J. Phys. Chem. C* **2013**, *117*, 23858–23867.
28. Marikutsa, A.V.; Rumyantseva, M.N.; Konstantinova, E.A.; Shatalova, T.B.; Gaskov, A.M. Active sites on nanocrystalline tin dioxide surface: effect of palladium and ruthenium oxides clusters. *J. Phys. Chem. C* **2014**, *118*, 21541–21549.
29. Frank, K.; Magapu, V.; Schindler, V.; Kohler, H.; Keller, H.B.; Seifert, R. Chemical analysis with tin oxide gas sensors: Choice of additives, method of operation and analysis of numerical signal. *Sens. Lett.* **2008**, *6*, 908–911.